ACS SENSORS

Letter

Cite This: ACS Sens. 2019, 4, 1980−1985

pubs.acs.org/acssensors

Dynamic Control of Peptide Strand Displacement Reaction Using Functional Biomolecular Domain for Biosensing

Yifan Dai,*[,†] Kevin Abbasi,[‡] Smarajit Bandyopadhyay,[§] and Chung Chiun Liu*[,†]

[†]Department of Chemical and Biomolecular Engineering and Electronics Design Center, and [‡]Department of Materials Science and Engineering, Case Western Reserve University, Cleveland, Ohio 44106, United States

[§]Lerner Research Institute, Cleveland Clinic, Cleveland, Ohio 44106, United States

Supporting Information

ABSTRACT: Nature's great repository provides nucleic acids and amino acids as the fundamental elements of life. Inspired by the programmability of nucleic acids, DNA nanotechnology has been extensively developed based on the strand displacement reaction of nucleic acids. In comparison with nucleic acids, amino acids possess higher programmability and more functionalities owing to the diversity of the amino acid unit. However, the design of the peptide-based bimolecular cascade is still limited. We herein describe a peptide-based strand displacement reaction, which was granted with a specific biological function by addition of a functional domain onto the coiled-coil peptide based displacement substrate. The displacement substrate was specifically designed to response to Tau protein based on a well-established Tau inhibition sequence. We demonstrated that the kinetics of the designed displacement reaction can be dynamically tuned through blocking the toehold region to prevent migration. A nanomolar Tau detection linear range was achieved through the designed displacement reaction within a rapid turnaround time of 30 min. We also presented the capability of the peptide strand displacement based sensing system operating in real human biological samples and its excellent orthogonality on response to irrelevant biological components. We envision that this will be of especially high utility for the development of next-generation biotechnology.

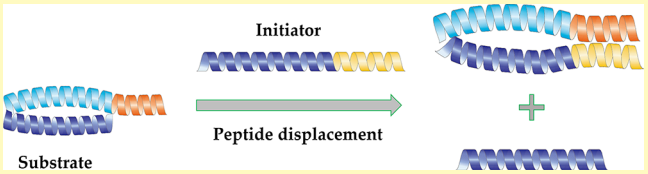

KEYWORDS: *peptide displacement reaction, electrochemical biosensor, coiled-coil, Tau detection, biomolecular motor*

The role of DNA as a powerful repository for genetic information storage greatly depends on its inherent stability from the hybridization of Watson−Crick base pairs.[1] Inspired by the programmability of nucleic acid hybridization created by Nature, DNA nanotechnology becomes a versatile and directable tool for the development of programmable logic gate, nonenzymatic biocatalysis, biomolecular motors, biosensors, and controllable synthesis of nanostructures.[2−7] The fundamental basis of the nucleic acid tool box is the programmable strand displacement reaction, which has been extensively evaluated and developed owing to the regularity of nucleic acid hybridization.[2,8,9] Especially for biosensor application, the high controllability and programmability of the nucleic strand displacement reaction provide various designs of nonenzymatic, target triggered, signal-on assays, enhancing the detection sensitivity and accuracy.[10−13] For example, the target triggered strand displacement reaction was initially applied to induce the change of electron tunneling length for certain redox probes on the sensor surface, achieving rapid detection of the target.[14] Furthermore, the strand displacement reaction was applied to initiate a dramatic change of the surface charge on the biosensor for the development of a universal sensing system for the detection of all types of analytes.[15] These systems demonstrated the high applicability of the nucleic acid based strand displacement on biosensor development. Other than nucleic acid, another great fundamental composition produced by nature is the amino acid, which can be granted various biological functions directly by sequence design for diverse applications, such as polymer networks, nanostructure synthesis, and biomarker inhibitors.[16−20] Therefore, a programmable peptide nanotechnology can be extremely valuable and highly functionalizable for more diverse biological tool developments. However, the study of programmable biomolecular devices based on the utilization of amino acids is rather limited.[21] Inspired by the widely developed nucleic acid strand displacement, we herein demonstrate the use of peptide interaction modules to construct programmable biomolecular motors through the peptide strand displacement reaction. The constructed peptide displacement reaction was characterized by an on-chip electrochemical analysis and further developed as a biosensing strategy for Tau protein detection.

The fundamental basis of the DNA strand displacement reaction is the hybridization of nucleic acid base pairs (A-T/C-G) through hydrogen bonding and the hybridization induced thermal dynamics driving, mostly enthalpy driving.[22,23] To imitate the hydrogen bond based hybridization of nucleic acid base pairs to construct peptide-based strand displacement, the

Received: May 6, 2019
Accepted: July 16, 2019
Published: July 16, 2019

DOI: 10.1021/acssensors.9b00831
ACS Sens. 2019, 4, 1980−1985

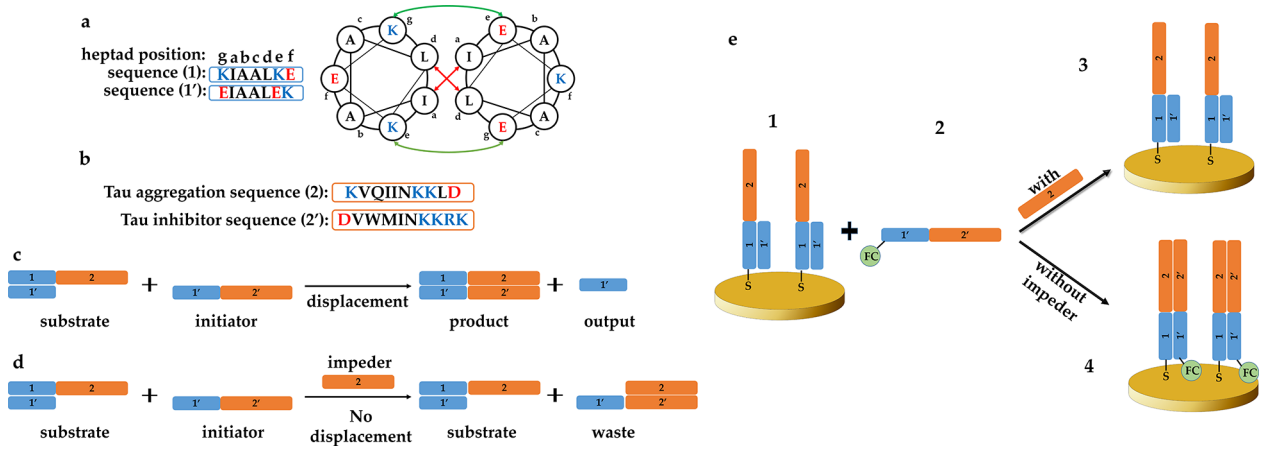

Figure 1. (a) Amino acid squences of the heterodimeric helical heptad coiled-coils; helical wheel representation of electrostatic (green) and hydrophobic (red) interaction between heterodimers (coiled-coil viewed in cross-section). (b) Amino acid sequences of the functional domain based on Tau protein aggregation region and corresponding impeder (inhibitor) peptide. (c) Peptide displacement reaction based on a substrate (with exposed domain 2) and an initiator as the fuel for the displacement reaction. (d) Dynamic manipulation of the peptide displacement reaction through an impeder peptide, blocking the initiator from the displacement reaction. (e) Substrate complex immobilized on the gold working electrode and the following displacement resulted surface biomolecule differences based on the condition of with/without the impeder.

electrostatic interaction between oppositely charged amino acids can be applied, such as formation of the coiled-coil helix.[24] Therefore, two complementary heptad coiled-coil peptides were applied in this study as the bases for the strand displacement reaction design (Figure 1a). Specifically, two triplet repeats of the heptad coiled-coils were applied to form the DNA-like helix as one domain of the displacement substrate. Furthermore, in order to functionalize this biomolecular motor as a Tau biosensor, a structure-based peptide impeder for Tau aggregation was added as a second domain (Figure 1b).[25] With the addition of the second domain, we granted this coiled-coil based substrate a binding motif (2') to interact with a specific region of Tau protein (Tau aggregation sequence (2)), which was recognized to form aggregates as a sign of neurodegenerative disorders.[25,26] Thus, we applied this combined peptide sequences as a biomolecular motor to examine the binding behavior of the Tau protein inhibition pairs (2−2′) and further utilized this motor as an autonomous and controllable biosensing strategy for Tau protein detection. Specifically, the electrochemistry based biosensor was selected for development of the biosensing system, owing to the high sensitivity, cost-effectiveness, and time-efficiency of the electrochemical transduction process.[27−32]

The principle design of the peptide strand displacement reaction is illustrated in Figure 1c. A substrate peptide strand was designed with coiled-coils hybridization sequences (1-1') and a toehold sequence (2), which was a functional domain. Building upon the substrate strand, the strand displacement was initiated by an initiator strand (1′−2′, which functioned as the fuel for the displacement reaction). The displacement reaction was completed with a hybridized product based on the binding interaction between 1-2 and 1′−2′ with an output strand 1′ from the initial substrate. Moreover, the second domain can be utilized to independently control the dynamics of the displacement reaction as shown in Figure 1d. With the addition of the impeder strand 2, the initiator 2′ domain was blocked and a waste was generated. Consequently, the fuel would no longer be supplied to trigger the displacement reaction. By introduction of the impeder, we can achieve selective deactivation of the strand displacement process, enriching the toolbox of the peptide displacement reaction design.

To examine these concepts and demonstrate this programmable biomolecular motor for biosensor application, a biomolecular circuit was constructed on an electrochemical sensor as shown in Figure 1e. The electrochemical sensor was a three-electrode system with gold working and counter electrodes and a Ag/AgCl reference electrode. The detailed configuration and characterization of this three-electrode system was described in a previous study.[33] In order to perform the on-chip analysis of the displacement reaction, the peptide (1−2) was designed with a cysteine linker for immobilization onto the gold electrode through the Au−S bond. After incubation of 20 μL of 35 μM peptide (1−2) for 2 h at room temperature to form the self-assembled peptide layer, time-of-flight secondary ion mass spectroscopy was applied to confirm the formation of the Au−S bond (Figure S1a). Electrochemical stripping analysis was then performed to quantify the amount of Au−S bond desorbed in order to acquire the amount of peptide (1−2) tethered on the electrode. As shown in Figure S1b, the amount of peptide immobilized on the electrode was around 980 pmol per working electrode. 3.5 μM of peptide (1′) was then incubated to hybridize with peptide (1−2) to form the displacement substrate complex onto the gold electrode (Figure 1e-1). The optimization of the on-chip hybridization time was evaluated by electrochemical impedance spectroscopy (EIS) using redox probe $[Ru(NH_3)_6]^{2+/3+}$ (Figure S2). The EIS results demonstrated a saturation of signal after hybridization time over 25 min, which was then selected as an optimized time for the formation of the displacement substrate complex (1−2−1′). After the formation of the substrate, 20 μL of 350 nM (amount of 7 pmol) of the initiator strand was incubated onto the substrate complex covered electrode for 1 h, which was sufficient to reach the displacement reaction equilibrium as demonstrated by a previous study.[21] To evaluate the peptide displacement concept, EIS was first applied to examine the electrode surface impedance change during the displacement process. As shown in Figure 2a, an increase of surface

DOI: 10.1021/acssensors.9b00831
ACS Sens. 2019, 4, 1980−1985

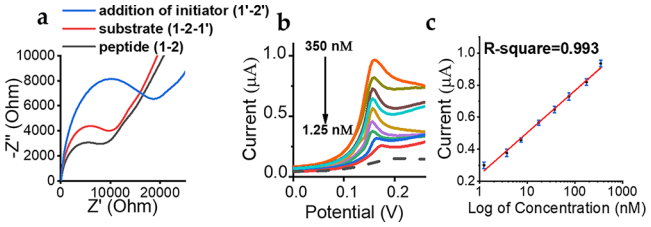

Figure 2. Proof-of-concept electrochemical evaluation: (a) EIS evaluation of step-by-step surface impedance change of the strand displacement reaction. (b) DPV evaluation of the ferrocene oxidation reaction before and after introduction of different concentrations of ferrocene linked initiator onto the substrate complex covered electrode. (c) Linear calibration curve of different concentrations of initiator against the current outputs based on the electrochemical signal of ferrocene.

impedance (R_{ct}) was observed throughout the substrate formation to the addition of initiator due to the bigger size of the initiator strand (1'-2') compared with that of the peptide strand (1′). Moreover, it was critical to confirm that the designed initiator (1′−2′) displaced the strand (1′) from the substrate completely during the strand displacement reaction, instead of forming a trimer by binding initiator through the formation of 2−2′ domain as well as maintaining the strand (1′) on the substrate (Figure S3a). Therefore, EIS was conducted to evaluate the surface impedance based on strand (1−2) directly hybridized with initiator strand (1′−2′). As shown in Figure S3b, the direct hybridization resulted in an EIS curve overlaid with that of the strand displacement formed surface (same as the blue line in Figure 2a), confirming that the introduction of initiator successfully induced and completed the strand displacement reaction through displacing the strand (1′) as an output. Circular dichroism (CD) was also applied to confirm the displacement principle and evaluate the change of the secondary structure before and after the displacement reaction. In order to evaluate the secondary structure of the peptide complex (1−2−1′−2′) after the displacement reaction, centrifuge filtration by Amicon-5k tube was applied to remove the remaining displaced output (1′). As shown in Figure S4, CD demonstrated the α-helix secondary structure of both peptides based on two negative bands at 222 and 208 nm and a positive band at 193 nm. However, by comparing the ellipticity $[\theta]_{222}$ (which is directly proportional to the amount of residues in a helix[34]) between the two peptides, the displacement substrate complex (1−2−1′) demonstrated a partial α-helix secondary structure and the displacement product (1−2−1′−2′) demonstrated a more comprehensive α-helix secondary structure. These results verified the validity of the designed peptide displacement reaction.

To obtain direct evidence of the displacement reaction in order to further apply to development of electrochemical biosensor, the initiator strand (1′−2′) was linked with a ferrocene probe to generate an electrochemical signal. Different concentrations of initiator strands were incubated onto the substrate covered electrode for 1 h to achieve displacement equilibrium. After incubation, the electrodes were washed and dried to remove the remaining non-hybridized biomolecules. Differential pulse voltammetry (DPV) was then applied to evaluate the ferrocene oxidation reaction. As shown in Figure 2b, a significant oxidation peak at around 0.16 V (vs Ag/AgCl) was observed with the introduction of the initiator (comparing with the response from the substrate only (black dashed line)), indicating the success of the strand displacement reaction. A dynamic range of the initiator concentration was observed from 1.25 nM to 350 nM, covering an effective displacement concentration range over 2 orders of magnitude. A low limit of initiator concentration was observed at 0.35 nM (red line). Figure 2c demonstrated the linear calibration curve of the DPV current outputs against different concentrations (1.25−350 nM) of the initiators ($Y = 0.262X + 0.241$) with an R^2 value of 0.993 and a RSD value at 2.51%, indicating an excellent reproducibility and stability of the designed peptide displacement reaction.

After confirming the principle concept of the peptide molecular motor through electrochemical analysis of the displacement reaction process, the kinetic performance of the peptide displacement was investigated. Three different concentrations of initiator were tested on the substrate complex covered electrode array. DPV measurement was conducted every 180 s as an individual event. The obtained current output was converted into the concentration of the product (1−2−1′−2′) by the calibration curve obtained from Figure 2c. The kinetics equation was formulated and derived as a pseudo-first-order equation owing to the fact that the experimental substrate concentration was over 2 orders of magnitude larger than the initiator concentration (SI Text S3).[35] As shown in Figure 3a, different concentrations of

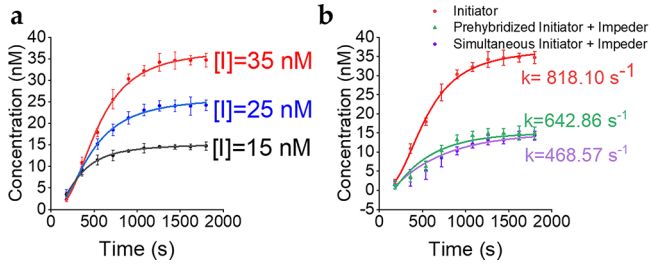

Figure 3. (a) Rate constant fitting of the peptide displacement process based on different concentrations of initiator strand. (b) Dynamic control of the kinetics of the peptide strand displacement reaction by introduction of impeder (20 nM) into the system through the prehybridization interaction with the initiator before the displacement reaction or simultaneously interacting with initiator during the displacement reaction.

initiator were tested by the substrate covered electrode over 2000 s. A saturation of signal was observed after 1000 s. The kinetic constants of different concentrations of initiator induced displacement reaction were fitted by Equation S3 as shown in Figure S5 and yielded a kinetic constant of 818.10 s^{-1}.

In order to demonstrate the kinetic control of this peptide displacement process, we introduced an impeder into the displacement reaction. The impeder (2) was designed to specifically bind with the second domain (2') (functional domain) of the initiator. Therefore, upon the introduction of the impeder, the kinetics of the peptide displacement reaction would be altered. We first evaluated the kinetics based on the prehybridized (30 min) impeder strand (20 nM) and initiator strand (35 nM). As shown in Figure 3b (green line), the addition of prehybridized impeder initiator complex reduced the amount of active initiator in the incubation solution to 15 nM. A decreased kinetic constant was observed. We believed that the reduced kinetic constant was affected by the increased

DOI: 10.1021/acssensors.9b00831
ACS Sens. 2019, 4, 1980−1985

biomolecular complexity in the incubation sample, therefore decreasing the diffusion of the active initiators. Moreover, to demonstrate that the peptide displacement process can be dynamically controlled, we coincubated the impeder strand (20 nM) and the initiator strand (35 nM) simultaneously. The purple line presented a significant decrease of kinetic constant by 42.7% compared with the kinetic constant based on only initiator. These tests demonstrated that the kinetics of the designed peptide strand displacement reaction can be dynamically tuned through the addition of an impeder strand, reducing the efficiency of the hybridization and migration processes between the initiator and the substrate.

The dynamic control strategy of the functionalized peptide strand displacement can be further utilized in biosensor development. We applied the designed peptide displacement for the detection of Tau protein, which is a biomarker of neurodegenerative disorders.[36,37] The impeder sequence (2) was a fragment of Tau protein, which served as the detection target. The second domain (2') of the initiator sequence was a Tau inhibition sequence, which was confirmed to be able to specifically recognize and bind full-length Tau protein.[25] Human Tau protein was then applied as the impeder for the strand displacement reaction. First, different concentrations of Tau protein were prehybridized with the 350 nM initiator strand for 30 min at 37 °C. After hybridization, the sample was incubated onto the displacement substrate covered electrode for 20 min prior to the DPV test. As shown in Figure 4a, a DPV detection range of Tau protein from 10 nM to 300 nM was obtained. Theoretically, 10 nM to 300 nM of Tau protein corresponded with the current outputs based on 340 nM to 50 nM of initiator strand. However, the current output (Figure 4a) based on the impeder as full-length Tau (43 kDa) compared with the current output (Figure 2b) based on impeder as fragment Tau (1.3 kDa) was significantly decayed by around 30%. This phenomenon may be explained as the size of full-length Tau being around 30 times bigger than the fragment Tau; therefore it may decrease the kinetics of the peptide strand displacement reaction due to the complex matrix produced by the presence of full length Tau. Also, the presence of a bigger protein might increase the steric hindrance effect, impeding the effective hybridization and decreasing the effective strand displacement reaction. Even though a decrease of the dynamic displacement reaction range was observed, a linear calibration curve was still obtained as $Y = -0.0013X + 0.6082$ with an R^2 value of 0.985 based on the Tau protein concentration of 10 nM to 300 nM. A detection limit was observed as 0.3 nM (red line in Figure 4a).

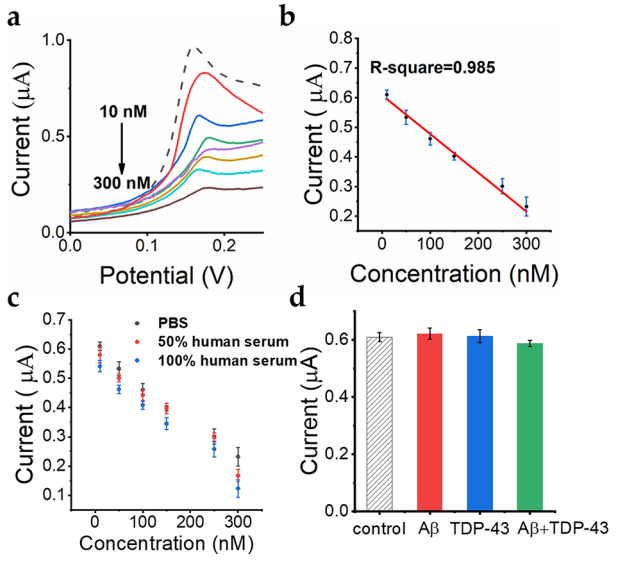

Figure 4. (a) DPV responses of different Tau protein concentrations in 0.1 M PBS solution hybridized with 350 nM of initiator resulted strand displacement reaction. Black dashed line was obtained based on the zero Tau protein concentration as the baseline. Red line was observed as the detection limit of Tau protein for 0.3 nM. (b) Linear calibration of Tau protein concentration (10−300 nM) against current outputs of ferrocene signal (n = 3). (c) Current responses comparison between different biological buffers for Tau sample preparation. (d) Evaluation of the orthogonality of the designed the peptide strand displacement reaction.

To evaluate the detection performance of this peptide displacement in response to complex human matrices, 50% and 100% pooled healthy human serum were utilized for human Tau protein sample preparation. As shown in Figure 4c, compared with the detection response of Tau protein sample prepared in PBS solution, the detection response of the sample prepared in 50% human serum and 100% human serum decreased on average by 12% and 19%, respectively, which was an acceptable signal influence from the matrix effect. We believed that the decrease of the ferrocene signal was caused by the increased sample complexity leading to a decrease in diffusion rate; therefore, less ferrocene conjugated initiator completed the displacement reaction. However, the same detection range and detection limit were still achieved in complex matrices.

Moreover, it was critical to examine the orthogonality of the biomolecular motor, evaluating the level of unwanted crosstalk from irrelevant biological components, which may hinder the construction of more complex biological circuits and decrease the motor operating efficiency. β-Amyloid 1−40 protein and TAR DNA binding protein 43 were selected as impeders to evaluate the orthogonality of the displacement system, because these two proteins are recognized as important biomarkers for neurodegenerative disorders and are also co-functioned in cerebrospinal fluid with Tau protein.[38,39] As shown in Figure 4d, control was based on the current output from only 10 nM of the Tau protein as an impeder interacting with the initiator. A solution containing 10 nM of Tau protein and 5 nM of β-amyloid 1−40 (red), a solution containing 10 nM of Tau protein and 5 nM of TAR DNA binding protein 43 (blue), and a solution containing 10 nM of Tau protein, 5 nM of β-amyloid 1−40, and 5 nM of TAR DNA binding protein 43 were individually incubated with the 350 nM initiator strand for 30 min at 37 °C allowing hybridization between the impeder and the initiator. After hybridization, the solution was directly incubated onto the substrate-covered electrode for 30 min prior to the DPV test. The interference substances demonstrated a signal variation of around 3.5%, which was slightly over the RSD of the control (2.5%), demonstrating an acceptable selectivity for the designed peptide strand displacement. These experiments proved that the designed peptide strand displacement reaction is feasible in the complex biological environment, indicating the great potential of the peptide displacement concept for diverse biological applications. Also, evaluation of the orthogonality of the designed system demonstrated its applicability for further development of more complex biological systems.

DOI: 10.1021/acssensors.9b00831
ACS Sens. 2019, 4, 1980−1985

It is also necessary to mention that the coiled-coil helix interaction is strongly sequence-dependent, and therefore the combination of peptide strands might be limited. However, by enhancing the understanding of peptide interaction pairs with controllable secondary structures, we believe that future researchers can build on this peptide displacement concept to generate more diverse and applicable biomolecular circuits using different types of peptides for various biotechnology applications, providing the scientific impact similar to that brought by nucleic acid strand displacement into the community.

In conclusion, we developed and demonstrated a peptide-based strand displacement reaction with tunable kinetic performance, capability of operating in complex biological matrices, and an excellent orthogonality. The designed peptide displacement substrate included a coiled-coil peptide basis as the migration sequence and a functional peptide domain as the toehold sequence to initiate the strand displacement reaction. By attaching a functional domain onto the initiator strand, we granted the stand displacement reaction a specific biological function. Our presentation first demonstrated that the peptide displacement reaction can be dynamically controlled by the introduction of an impeder. Also, the designed peptide displacement reaction can effectively function as a biomolecular motor for biotechnology applications in complex biological matrices. Comparing with conventional nucleic acid based strand displacement, peptide-based strand displacement possesses greater potential for versatile biological applications owing to the higher diversity of the amino acid units. Based on this novel concept, future researchers will be able to apply differently designed peptide displacement mechanisms to perform valuable bioengineering applications, such as biosensing, logic gate design, and drug delivery.

■ ASSOCIATED CONTENT

Supporting Information

The Supporting Information is available free of charge on the ACS Publications website at DOI: 10.1021/acssensors.9b00831.

Materials and apparatus; Experimental Section; TOF secondary ion mass spectroscopy; EIS measurement; Illustration of incomplete peptide strand displacement reaction; CD evaluation; Dynamic kinetic model for peptide strand displacement reaction (PDF)

■ AUTHOR INFORMATION

Corresponding Authors

*E-mail: yxd176@case.edu.
*E-mail: cxl9@case.edu.

ORCID

Yifan Dai: 0000-0002-1009-5790
Chung Chiun Liu: 0000-0002-4313-8064

Notes

The authors declare no competing financial interest.

■ ACKNOWLEDGMENTS

We acknowledge the support of Wallace R. Persons Research Fund from Case Alumni Association. We also greatly appreciate Xintong Cao for the creation of artwork for this manuscript. Experimental support from Electronics Design Center of Case Western Reserve University is also acknowledged.

■ REFERENCES

(1) Pinheiro, A. V.; Han, D.; Shih, W. M.; Yan, H. Challenges and opportunities for structural DNA nanotechnology. *Nat. Nanotechnol.* **2011**, *6* (12), 763−772.

(2) Chen, R. P.; Blackstock, D.; Sun, Q.; Chen, W. Dynamic protein assembly by programmable DNA strand displacement. *Nat. Chem.* **2018**, *10* (4), 474−481.

(3) Peng, R.; Zheng, X.; Lyu, Y.; Xu, L.; Zhang, X.; Ke, G.; Liu, Q.; You, C.; Huan, S.; Tan, W. Engineering a 3D DNA-Logic Gate Nanomachine for Bispecific Recognition and Computing on Target Cell Surfaces. *J. Am. Chem. Soc.* **2018**, *140* (31), 9793−9796.

(4) Porchetta, A.; Ippodrino, R.; Marini, B.; Caruso, A.; Caccuri, F.; Ricci, F. Programmable Nucleic Acid Nanoswitches for the Rapid, Single-Step Detection of Antibodies in Bodily Fluids. *J. Am. Chem. Soc.* **2018**, *140* (3), 947−953.

(5) Li, F.; Zhang, H.; Wang, Z.; Li, X.; Li, X.-F.; Le, X. C. Dynamic DNA Assemblies Mediated by Binding-Induced DNA Strand Displacement. *J. Am. Chem. Soc.* **2013**, *135* (7), 2443−2446.

(6) Tan, Z.; Feagin, T. A.; Heemstra, J. M. Temporal Control of Aptamer Biosensors Using Covalent Self-Caging To Shift Equilibrium. *J. Am. Chem. Soc.* **2016**, *138* (20), 6328−6331.

(7) Petersen, P.; Tikhomirov, G.; Qian, L. Information-based autonomous reconfiguration in systems of interacting DNA nanostructures. *Nat. Commun.* **2018**, *9* (1), 5362.

(8) Yang, X.; Tang, Y.; Traynor, S. M.; Li, F. Regulation of DNA Strand Displacement Using an Allosteric DNA Toehold. *J. Am. Chem. Soc.* **2016**, *138* (42), 14076−14082.

(9) Green, A. A.; Silver, P. A.; Collins, J. J.; Yin, P. Toehold Switches: De-Novo-Designed Regulators of Gene Expression. *Cell* **2014**, *159* (4), 925−939.

(10) Massey, M.; Medintz, I. L.; Ancona, M. G.; Algar, W. R. Time-Gated FRET and DNA-Based Photonic Molecular Logic Gates: AND, OR, NAND, and NOR. *ACS Sensors* **2017**, *2* (8), 1205−1214.

(11) Liu, Y.; Shen, T.; Li, J.; Gong, H.; Chen, C.; Chen, X.; Cai, C. Ratiometric Fluorescence Sensor for the MicroRNA Determination by Catalyzed Hairpin Assembly. *ACS Sensors* **2017**, *2* (10), 1430−1434.

(12) Yang, F.; Li, Q.; Wang, L.; Zhang, G.-J.; Fan, C. Framework-Nucleic-Acid-Enabled Biosensor Development. *ACS Sensors* **2018**, *3* (5), 903−919.

(13) Li, L.; Xiao, X.; Ge, J.; Han, M.; Zhou, X.; Wang, L.; Su, X.; Yu, C. Discrimination Cascade Enabled Selective Detection of Single-Nucleotide Mutation. *ACS Sensors* **2017**, *2* (3), 419−425.

(14) Lubin, A. A.; Plaxco, K. W. Folding-Based Electrochemical Biosensors: The Case for Responsive Nucleic Acid Architectures. *Acc. Chem. Res.* **2010**, *43* (4), 496−505.

(15) Das, J.; Cederquist, K. B.; Zaragoza, A. A.; Lee, P. E.; Sargent, E. H.; Kelley, S. O. An ultrasensitive universal detector based on neutralizer displacement. *Nat. Chem.* **2012**, *4*, 642−648.

(16) Couet, J.; Samuel, J. J. S.; Kopyshev, A.; Santer, S.; Biesalski, M. Peptide−polymer hybrid nanotubes. *Angew. Chem., Int. Ed.* **2005**, *44* (21), 3297−3301.

(17) Gazit, E. Self-assembled peptide nanostructures: the design of molecular building blocks and their technological utilization. *Chem. Soc. Rev.* **2007**, *36* (8), 1263−1269.

(18) Nile, A. H.; e Melo, F. d. S.; Mukund, S.; Piskol, R.; Hansen, S.; Zhou, L.; Zhang, Y.; Fu, Y.; Gogol, E. B.; Kömüves, L. G.; et al. A selective peptide inhibitor of Frizzled 7 receptors disrupts intestinal stem cells. *Nat. Chem. Biol.* **2018**, *14* (6), 582−590.

(19) Upadhyaya, P.; Qian, Z.; Selner, N. G.; Clippinger, S. R.; Wu, Z.; Briesewitz, R.; Pei, D. Inhibition of Ras signaling by blocking Ras−effector interactions with cyclic peptides. *Angew. Chem., Int. Ed.* **2015**, *54* (26), 7602−7606.

(20) Owens, A. E.; de Paola, I.; Hansen, W. A.; Liu, Y.-W.; Khare, S. D.; Fasan, R. Design and Evolution of a Macrocyclic Peptide Inhibitor

DOI: 10.1021/acssensors.9b00831
ACS Sens. 2019, 4, 1980−1985

of the Sonic Hedgehog/Patched Interaction. *J. Am. Chem. Soc.* **2017**, *139* (36), 12559−12568.
(21) Gröger, K.; Gavins, G.; Seitz, O. Strand Displacement in Coiled-Coil Structures: Controlled Induction and Reversal of Proximity. *Angew. Chem., Int. Ed.* **2017**, *56* (45), 14217−14221.
(22) Demidov, V. V.; Protozanova, E.; Izvolsky, K. I.; Price, C.; Nielsen, P. E.; Frank-Kamenetskii, M. D. Kinetics and mechanism of the DNA double helix invasion by pseudocomplementary peptide nucleic acids. *Proc. Natl. Acad. Sci. U. S. A.* **2002**, *99* (9), 5953−5958.
(23) Zhang, D. Y.; Winfree, E. Control of DNA strand displacement kinetics using toehold exchange. *J. Am. Chem. Soc.* **2009**, *131* (47), 17303−17314.
(24) Fletcher, J. M.; Harniman, R. L.; Barnes, F. R.; Boyle, A. L.; Collins, A.; Mantell, J.; Sharp, T. H.; Antognozzi, M.; Booth, P. J.; Linden, N.; et al. Self-assembling cages from coiled-coil peptide modules. *Science* **2013**, *340* (6132), 595−599.
(25) Seidler, P.; Boyer, D.; Rodriguez, J.; Sawaya, M.; Cascio, D.; Murray, K.; Gonen, T.; Eisenberg, D. Structure-based inhibitors of tau aggregation. *Nat. Chem.* **2018**, *10* (2), 170−176.
(26) Sievers, S. A.; Karanicolas, J.; Chang, H. W.; Zhao, A.; Jiang, L.; Zirafi, O.; Stevens, J. T.; Münch, J.; Baker, D.; Eisenberg, D. Structure-based design of non-natural amino-acid inhibitors of amyloid fibril formation. *Nature* **2011**, *475*, 96−100.
(27) Dai, Y.; Chiu, L.-Y.; Chen, Y.; Qin, S.; Wu, X.; Liu, C. C. Neutral Charged Immunosensor Platform for Protein-based Biomarker Analysis with Enhanced Sensitivity. *ACS Sensors* **2019**, *4* (1), 161−169.
(28) Kelley, S. O.; Mirkin, C. A.; Walt, D. R.; Ismagilov, R. F.; Toner, M.; Sargent, E. H. Advancing the speed, sensitivity and accuracy of biomolecular detection using multi-length-scale engineering. *Nat. Nanotechnol.* **2014**, *9* (12), 969−980.
(29) Labib, M.; Sargent, E. H.; Kelley, S. O. Electrochemical methods for the analysis of clinically relevant biomolecules. *Chem. Rev.* **2016**, *116* (16), 9001−9090.
(30) Dai, Y.; Liu, C. C. Recent Advances on Electrochemical Biosensing Strategies toward Universal Point of Care Systems. *Angew. Chem., Int. Ed.* **2019**, DOI: 10.1002/anie.201901879.
(31) Das, J.; Ivanov, I.; Montermini, L.; Rak, J.; Sargent, E. H.; Kelley, S. O. An electrochemical clamp assay for direct, rapid analysis of circulating nucleic acids in serum. *Nat. Chem.* **2015**, *7*, 569−575.
(32) Dai, Y.; Huang, J.; Zhang, H.; Liu, C. C. Highly sensitive electrochemical analysis of tunnel structured MnO2 nanoparticle-based sensors on the oxidation of nitrite. *Sens. Actuators, B* **2019**, *281*, 746−750.
(33) Dai, Y.; Wang, C.; Chiu, L.-Y.; Abbasi, K.; Tolbert, B. S.; Sauvé, G.; Yen, Y.; Liu, C.-C. Application of bioconjugation chemistry on biosensor fabrication for detection of TAR-DNA binding protein 43. *Biosens. Bioelectron.* **2018**, *117*, 60−67.
(34) Hirst, J. D.; Brooks, C. L. Helicity, Circular Dichroism and Molecular Dynamics of Proteins. *J. Mol. Biol.* **1994**, *243* (2), 173−178.
(35) Li, M.-X.; Xu, C.-H.; Zhang, N.; Qian, G.-S.; Zhao, W.; Xu, J.-J.; Chen, H.-Y. Exploration of the Kinetics of Toehold-Mediated Strand Displacement via Plasmon Rulers. *ACS Nano* **2018**, *12* (4), 3341−3350.
(36) Wittmann, C. W.; Wszolek, M. F.; Shulman, J. M.; Salvaterra, P. M.; Lewis, J.; Hutton, M.; Feany, M. B. Tauopathy in Drosophila: neurodegeneration without neurofibrillary tangles. *Science* **2001**, *293* (5530), 711−714.
(37) Clavaguera, F.; Bolmont, T.; Crowther, R. A.; Abramowski, D.; Frank, S.; Probst, A.; Fraser, G.; Stalder, A. K.; Beibel, M.; Staufenbiel, M.; et al. Transmission and spreading of tauopathy in transgenic mouse brain. *Nat. Cell Biol.* **2009**, *11* (7), 909−913.
(38) Chen-Plotkin, A. S.; Lee, V. M.-Y.; Trojanowski, J. Q. TAR DNA-binding protein 43 in neurodegenerative disease. *Nat. Rev. Neurol.* **2010**, *6* (4), 211−220.
(39) Mawuenyega, K. G.; Sigurdson, W.; Ovod, V.; Munsell, L.; Kasten, T.; Morris, J. C.; Yarasheski, K. E.; Bateman, R. J. Decreased clearance of CNS β-amyloid in Alzheimer's disease. *Science* **2010**, *330* (6012), 1774.

DOI: 10.1021/acssensors.9b00831
ACS Sens. 2019, 4, 1980−1985